

Designed and Microfabricated a High-Precision Conductivity and Temperature Sensor for Marine Measurement

1.Behara Sai Karthik 2.M.V.N.Sankaram 3.Duddu Hemanth Kumar

Department of Marine Engineering,
Andhra University,
Visakhapatnam , AP, INDIA.

Abstract:

Precise meshing and three-dimensional monitoring of the marine environment are very important for marine resources exploration, fishery development, and military activities. Therefore, a high-precision, low power consumption, low-cost and multiparameter integrated miniaturized sensor has been in a large-scale demand. Besides, conductivity and temperature are the basic dynamic parameters of the ocean. This paper presents a high-precision conductivity and temperature (CT) integrated sensor based on the micro-electro-mechanical system (MEMS) batch microfabrication technology, which has small size, low cost, high uniformity, and efficiency in meshing and three-dimensional marine measurements. In this study, the miniaturized CT sensor showed excellent linearity of conductivity ($R^2 \geq 0.99999$) and temperature ($R^2 \geq 0.999$) measurements. The temperature sensitivity of the CT sensor is $0.0619 \text{ }^\circ\text{C}/\Omega$, and the cell constant of the CT sensor is 2.559 cm^{-1} . The temperature test also shows the high repeatability with the variance coefficient of 0.6%. Furthermore, it shows an excellent consistency for batch. The coefficient of variance of cell constants is $\pm 0.019 \text{ cm}^{-1}$ and the 95% confidence intervals for the conductivity is demonstrated to be $\pm 0.0048 \text{ mS/cm}$. The variance coefficient of the temperature sensor is only 1.8%. The results indicate that the batch microfabricated sensors are suitable for a large-scale deployment in the Marine Internet of Things.

Key words: Batch microfabrication, CT miniaturized sensors, high precision, marine measurement.

INTRODUCTION:

Prompt: Rewrite the sentence about the importance of salinity and temperature measurements for marine applications.

Revised Sentence:

Salinity and temperature, fundamental variables in oceanography, are critical for accurate marine observations, climate modeling, and biological studies.

Explanation of changes:

Removed redundancies: The phrase "dynamic marine parameters" is redundant, as salinity and temperature are inherently marine variables.

Used more technical terms: "Oceanography" is a more specific term than "marine observation."

Emphasized the importance: The phrase "critical for" emphasizes the importance of these measurements.

This revised sentence is more concise, technically accurate, and effectively conveys the importance of salinity and temperature measurements in marine applications[1].

Revised Sentence: Salinity is determined from the measured electrical conductivity of seawater using a calibration based on 78 reference standards.

Explanation of changes:

Replaced "calculated from" with "determined from": This is a more technical term.

Added "calibration based on": This clarifies how the salinity is calculated from conductivity.

Used "reference standards" instead of "salt standards": This is a more precise term.

This revised sentence is more concise, technically accurate, and provides a clearer explanation of the process of determining salinity from conductivity [2]. A CTD (conductivity, temperature, depth) probe is the primary instrument for measuring these seawater parameters.

Explanation of changes:

Replaced "device" with "instrument": This is a more technical term.

Added "for measuring": This clarifies the function of the CTD probe.

Used "parameters" instead of "properties": This is a more general term that encompasses both salinity and temperature.

This revised sentence is more concise, technically accurate, and effectively describes the CTD probe as the primary tool for measuring seawater salinity, temperature, and depth[3].

Revised:

While commercial CTD sensors like the Seabird Series offer high-precision marine measurements, their size, cost, and power consumption limit their deployment in large-scale meshing and 3D environmental monitoring. To support modern fisheries and naval operations, abundant, precise marine data is crucial. In response, the Smart Ocean Planning initiative aims to...

Clarity and conciseness: The revised text is more direct and focused.

Technical accuracy: Terms like "deployment" and "3D environmental monitoring" are more precise.

Logical flow: The sentence structure better connects the challenges of CTD sensors with the need for more data.

Contextual relevance: The mention of "Smart Ocean Planning" is more naturally introduced.

This revised text provides a clearer and more concise overview of the challenges and needs related to CTD sensors and marine data[4-6].

Revised: The Ocean of Things (IoT) initiative demands the mass production of miniaturized CTD sensors at a reduced cost for widespread marine deployment. Recent research has increasingly concentrated on the miniaturization and integrated fabrication of these sensors.

Clarity and conciseness: The revised text is more direct and focused.

Technical accuracy: Terms like "Ocean of Things" and "integrated fabrication" are more precise.

Logical flow: The sentence structure better connects the need for miniaturized sensors with the ongoing research.

Contextual relevance: The reference to the Ocean of Things is more naturally introduced[10].

Revised: The Star-Oddi DST CTD, a compact salinity logger ideal for fish tagging, measures Ø17 mm x 46 mm and weighs 21 g. While it offers a small form factor, its conductivity accuracy (± 0.8 mS/cm) and temperature accuracy (± 0.1 °C) within their respective ranges may be insufficient for some applications. In contrast, Pedro M. Ramos et al. [11] proposed a four-terminal conductivity sensor constructed from a plastic tube with two internal ring electrodes to establish an electric field and two metallic probes to measure the resulting voltage.

Clarity and conciseness: The revised text is more direct and focused.

Technical accuracy: Terms like "conductivity accuracy" and "temperature accuracy" are used precisely.

Logical flow: The sentence structure better connects the advantages and limitations of the Star-Oddi DST CTD with the alternative design proposed by Ramos et al.

Contextual relevance: The comparison between the two sensors is more explicitly stated.

A fully integrated CMOS conductivity sensor, measuring 2.1 mm², incorporating four sensing electrodes and readout circuitry, was described for wet media. However, its detection range of 0.02 to 10 mS/cm falls short of ocean conductivity values, typically ranging from 5 to 70 mS/cm[12].

Clarity and conciseness: The revised text is more direct and focused.

Technical accuracy: Terms like "fully integrated CMOS" and "detection range" are used precisely.

Logical flow: The sentence structure better connects the sensor's features with its limitations.

Contextual relevance: The comparison to ocean conductivity is explicitly stated.

This revised text provides a clearer and more concise overview of the sensor's characteristics and its limitations for ocean applications[13].

Revised: A novel micro conductivity/temperature sensor fabricated via laser-induced graphene exhibited suboptimal linearity, with an R² value of approximately 0.99, as demonstrated in experimental data [14, 16].

Clarity and conciseness: The revised text is more direct and focused.

Technical accuracy: Terms like "laser-induced graphene" and "linearity" are used precisely.

Logical flow: The sentence structure better connects the sensor's fabrication method with its performance.

Contextual relevance: The reference to the experimental data is explicitly stated.

Revised:

MEMS technology, renowned for its miniaturization capabilities, has emerged as a promising approach for marine sensor development. Recent studies [17-26] have demonstrated the potential of MEMS-based CTD sensors, with Hyldgard et al. [23] achieving a compact 4 mm² sensor and Broadbent et al. [24] utilizing LCP thin-film technology. While these studies showcase the accuracy and miniaturization of MEMS sensors, additional metrics like sensitivity, response time, and repeatability are crucial for comprehensive evaluation. This work presents a novel MEMS-based CT sensor designed for batch fabrication, addressing these concerns. The proposed sensor exhibits exceptional consistency, precision, linearity, and sensitivity, making it well-suited for marine IoT applications and underwater observatory networks.

Clarity and conciseness: The revised text is more direct and focused.

Technical accuracy: Terms like "MEMS," "CTD," and "LCP" are used precisely.

Logical flow: The sentence structure better connects the advantages and limitations of MEMS-based sensors.

Contextual relevance: The reference to the need for additional evaluation metrics is explicitly stated.

Revised: The remaining sections of this paper are structured as follows: Section II outlines the operating principle and design of the micro CT sensor. Section III details the fabrication process and experimental setup. Section IV presents a thorough analysis of the proposed sensor. Finally, Section V summarizes our findings and conclusions.*

Clarity and conciseness: The revised text is more direct and focused.

Technical accuracy: The terms "operating principle," "fabrication process," and "comprehensive analysis" are more precise.

Logical flow: The sentence structure better connects the different sections of the paper.

This revised text provides a clearer and more concise overview of the paper's organization.

OPERATION PRINCIPLE AND DESIGN:

Operation Principle:

Revised:

Two primary conductivity sensor types employed in marine applications are inductive and electrode sensors [26]. While inductive sensors offer non-contact measurement to prevent corrosion, their complex structure and high cost hinder mass production and widespread deployment. Electrode sensors, fabricated using MEMS technology on silicon substrates, provide a more cost-effective and scalable alternative.

Clarity and conciseness: The revised text is more direct and focused.

Technical accuracy: Terms like "inductive sensors" and "electrode sensors" are used precisely.

Logical flow: The sentence structure better connects the advantages and limitations of the two sensor types.

Contextual relevance: The comparison between the two sensors is explicitly stated.

This revised text provides a clearer and more concise overview of the two main types of conductivity sensors used in marine applications, highlighting their respective advantages and disadvantages.

Revised:

Two common electrode sensor configurations for conductivity measurements are two-electrode and four-electrode cells, depicted in Figure 1. The equivalent circuit of each cell includes the solution resistance and the electrode-solution interface impedance. To accurately measure seawater resistance, this interface must be modeled. In a simple two-electrode sensor under DC excitation, polarization effects due to redox reactions and charging of the electrochemical double layer arise. These phenomena can be modeled using a Faradaic impedance (R_{ct} and Z_w) and a double layer capacitance (C_{dl}), respectively. The Faradaic impedance comprises a charge transfer resistance (R_{ct}) and a Warburg impedance (Z_w), with Z_w defined by [27]

Clarity and conciseness: The revised text is more direct and focused.

Technical accuracy: Terms like "electrode-solution interface," "polarization effects," and "Faradaic impedance" are used precisely.

Logical flow: The sentence structure better connects the different components of the equivalent circuit.

Contextual relevance: The reference to Figure 1 is explicitly stated.

This revised text provides a clearer and more concise overview of the two types of electrode sensors, their equivalent circuits, and the factors influencing the electrode-solution interface impedance.

$$Z_w = \sigma(w)0.5(1 - j) \quad (1)$$

Where σ is the Warburg coefficient, w is the radial frequency, and $j^2 = -1$.

Revised: DC excitation of the circuit can introduce measurement errors due to electrode polarization. To mitigate this, AC excitation at a suitable frequency is typically employed [28].

Clarity and conciseness: The revised text is more direct and focused.

Technical accuracy: Terms like "electrode polarization" and "AC excitation" are used precisely.

Logical flow: The sentence structure better connects the cause and effect of using DC excitation.

Revised:

The four-electrode sensor, unlike its two-electrode counterpart, mitigates electrode polarization by separating current and voltage electrodes. This configuration extends the measurable conductivity range and enhances measurement stability. As depicted in Figure 1(c), seawater resistance (R_s) is determined by applying AC current to the current electrodes and measuring the voltage drop between the voltage electrodes. The high input impedance of the voltage measurement circuit ensures negligible current flow through the voltage electrodes, eliminating the influence of R_{s1} and R_{s2} . Furthermore, the parasitic capacitance (C_p) is significantly reduced compared to two-electrode sensors, allowing for its neglect at appropriate AC frequencies.

Clarity and conciseness: The revised text is more direct and focused.

Technical accuracy: Terms like "electrode polarization," "four-electrode sensor," and "parasitic capacitance" are used precisely.

Logical flow: The sentence structure better connects the advantages of the four-electrode sensor to its underlying principles.

Contextual relevance: The reference to Figure 1(c) is explicitly stated.

This revised text provides a clearer and more concise explanation of the advantages of the four-electrode sensor over the two-electrode sensor, focusing on its ability to reduce electrode polarization and improve measurement accuracy.

The conductivity σ is related to the cell constant K , and the conductivity formula of the solution can be deduced as follows:

$$R_s = \frac{K}{\sigma} \quad (2)$$

In order to predict the performance of a conductivity cell, the cell constant K needs to be determined. According to the simple analytical approximation to the two planar electrodes model system [23], the cell constant K depends on the geometry of the conductivity cell, and it results in the simple exact expression:

Revised: For a given electrode length l and radius a , maximizing the inter-electrode distance d within a constrained

$$K = \frac{l}{\pi} \frac{\text{arccosh} \frac{a}{2a}}{2a} \quad (3)$$

chip area is crucial for optimizing the cell constant K . In the theoretical limit, the four-electrode cell constant approaches the two-electrode cell constant when the voltage electrodes are positioned close to the current electrodes and have minimal width.

Note: The term "cell constant" refers to a geometric factor that relates the measured conductivity to the actual conductivity of the solution. In this context, optimizing the cell constant ensures that the measured conductivity accurately reflects the true conductivity of the seawater.

Additionally, the temperature has a strong influence on the conductivity of the solution, and the relationship between conductivity (C_t) and temperature (T) is given by:

$$C_t = C_{cal} [1 + \alpha (T - T_{cal})] \quad (4)$$

Revised: Equation (4) compensates for temperature effects on conductivity, where C_t is the conductivity at temperature t , C_{cal} is the calibration conductivity at 25 °C, T_{cal} is the standard temperature, and α is the temperature coefficient. This work employs a platinum resistance thermometer (PRT) for seawater temperature measurement. Compared to conventional sensors like thermocouples, thermistors, and quartz thermometers, PRTs offer superior miniaturization, integration capabilities, a wider measurement range, enhanced stability, and lower cost, making them ideal for precision applications. As illustrated in the central part of Figure 1(c), temperature is determined by applying a fixed DC current.

Note: Equation (4) is likely a reference to a previously mentioned equation that details the temperature compensation calculation. The PRT's advantages over other temperature sensors are highlighted to justify its choice for this application. The method of temperature measurement using a fixed DC current is briefly explained.

Design:

As shown in Fig. 2(a), the CT sensor chip, with a size of 12 mm×12 mm×0.5 mm, is integrated with a four -electrode conductivity sensor and a thin-film platinum resistance temperature sensor.

Revised: The conductivity sensor directly interfaces with seawater due to the platinum electrodes' chemical inertness. A deposited silicon nitride (Si_3N_4) layer safeguards the temperature sensor from seawater exposure, leveraging its chemical stability and low water diffusion [9]. Epoxy glue seals the solder joints on the chip's periphery, isolating the wiring system from water during electrical connection to electronic equipment. This complete immersion of the CT sensor in the seawater environment enhances response time and measurement accuracy.

Note: The revised text provides a clearer and more concise explanation of the sensor's construction and the materials used to protect it from the seawater environment. The benefits of direct contact and the use of a protective layer are highlighted.

Revised: The electrode dimensions influence the cell constant K , which in turn affects the CT sensor's conductivity performance, as outlined in Equation (2). Similarly, the designed thin-film resistor's size impacts temperature measurement sensitivity. Following extensive testing and design iterations, the voltage electrode dimensions were finalized as 2.4 mm x 0.75 mm, with a 10 mm spacing between current electrodes. The platinum layer thickness is 300 nm, while a snake-shaped thin-film resistor with a 10.50 μm width serves as the temperature sensor, as depicted in Figure 2(b).

Note: The revised text provides a clearer and more concise explanation of the factors influencing the CT sensor's performance and the final design choices made for the electrodes and temperature sensor.

EXPERIMENTAL METHODS:

Fabrication Process of Integrated CT sensor:

Initially, the silicon wafer was thoroughly cleaned by washing it with H_2SO_4 : H_2O_2 = 7:1 (Step-1), NH_4OH : H_2O_2 : H_2O =1:1:7 (Step-2), HF : H_2O =1:50 (Step-2), and O_2 plasma treatment. Next, a double-side-polished 4-inch (100) crystal orientation silicon wafer with about 2- μm thick SiO_2 was obtained by the wet oxidation, as shown in Fig. 3(a). In Fig. 3(a), the oxide layer underlying the wafer is not shown. Further, the silicon wafer was thoroughly cleaned and dried and then coated with a 2.4- μm thick LC100A photoresist from Rohm and Haas by the EVG101 spin coater at the speed of 1000 r/min for 30 s. The proposed silicon wafer was exposed to a lithography machine for 15 s, and then immersed in the FHD-320 solution for 40 s for the purpose of patterning, as shown in Fig. 3(b).

Revised: The fabrication process for the CT sensor involved several steps: 1) a 300 nm thick Pt electrode was deposited using a lift-off process with a 30 nm Cr adhesion layer, as shown in Figures 3(c) and 3(d); 2) a 300 nm silicon nitride protective layer was deposited using PECVD (Figure 3(e)); 3) a patterned photoresist was created

using photolithography (Figure 3(f)); 4) the Si₃N₄ layer was selectively removed using RIE (Figure 3(g)); 5) the photoresist was removed using acetone (Figure 3(h)). The wafer was then diced into 34 individual chips, each packaged with a shielded wire and sealed with epoxy to ensure water resistance. This comprehensive process resulted in the fabrication of the integrated CT sensor.

Note: The revised text provides a clearer and more concise overview of the fabrication process, summarizing each step and referring to the relevant figures. The key materials and techniques used are highlighted, and the final product (the integrated CT sensor) is clearly stated.

Revised: The proposed CT sensor's performance was assessed for linearity, sensitivity, accuracy, repeatability, response time, detection range, and consistency. To calibrate the temperature sensor, it was immersed in a recirculating water bath (GH-30A, Xinzhi Company) with a temperature stability of ± 0.002 °C. This ensured both the sensor chip and the calibrated temperature sensor were subjected to identical temperature conditions.

Note: The revised text provides a clearer and more concise overview of the evaluation criteria and the calibration process used for the CT sensor. The specific equipment used for temperature control is mentioned, and the assumption of identical temperature conditions is explicitly stated.

Revised:

After stabilizing the water bath environment, the temperature sensor was evaluated using a Gamry electrochemical workstation. A fixed drive current of 10 μ A was applied to prevent sensor damage from excessive voltages. A sampling rate of 1 Hz was maintained over 200 seconds for each temperature point, with stable readings (resistance) averaged for accuracy. To assess response and recovery times, the sensor chip was rapidly transferred between an ice water mixture and a 30 °C water bath while monitoring its output. For conductivity cell calibration, reference solutions (6.16, 11.85, 33.10, and 101.00 mS/cm) were prepared using deionized water and KCl. A Gamry Reference 600+ workstation measured the conductivity cell's conductance in these solutions. Initial tests were conducted at room temperature without temperature compensation, using a 1 mA AC current source at 10 kHz to minimize double-layer and parasitic capacitance effects [31]. Each solution sample was measured for 200 seconds at a rate of 1 Hz. To evaluate consistency, five randomly selected sensor chips from the same wafer were tested for both conductivity and temperature.

Clarity and conciseness: The revised text is more direct and focused.

Technical accuracy: Terms like "recirculating water bath," "sampling rate," and "double-layer capacitance" are used precisely.

Logical flow: The sentence structure better connects the different experimental procedures and their purposes.

Contextual relevance: The reference to the Gamry electrochemical workstation is explicitly stated.

The experimental procedures used to evaluate the CT sensor's performance.

RESULTS AND DISCUSSION:

Temperature Sensor Performance:

Calibration:

Linearity: The sensor exhibited excellent linearity between measured resistance and predicted temperature, with R² values consistently exceeding 0.999.

Repeatability: High repeatability was demonstrated with a variance coefficient of 0.6%.

Sensitivity: The sensor's resistance and sensitivity were positively correlated.

Room Temperature Resistance: The sensor exhibited a room temperature resistance of over 5000 Ω , surpassing previously reported values.

Stability:

Temperature Stability: The sensor maintained a stable reading of 30.04 $^{\circ}\text{C}$ for 200 seconds, with a standard deviation of ± 0.01 $^{\circ}\text{C}$.

Accuracy: The error between the set temperature and the average reading was 0.04 $^{\circ}\text{C}$, indicating high temperature accuracy.

Batch Consistency:

Resistance and Temperature Relationship: A consistent relationship between resistance and temperature was observed across a batch of sensors.

Sensitivity: The average sensitivity of five sensors was 0.065 $^{\circ}\text{C}/\Omega$, with an average R^2 of 0.99953.

Variance: The variance coefficient was approximately 1.8% at each test point, demonstrating excellent consistency.

Intercept Variation: Variations in intercepts among sensors were attributed to minor dimensional deviations during fabrication, such as platinum thickness variations.

Response Time:

Rapid Response and Recovery: The sensor exhibited a fast response time of approximately 0.154 seconds and a short recovery time of 0.145 seconds.

Testing Conditions: The response time was evaluated under conditions simulating seawater temperature changes.

Conclusion:

The novel temperature sensor demonstrated exceptional performance in terms of linearity, repeatability, accuracy, and response time. These characteristics make it well-suited for applications in marine environments, where rapid temperature changes and high precision measurements are essential.

Conductivity Cell Performance:

As shown in Fig. 8, the maximum measurement error of the conductivity cell was ± 0.08 mS/cm, and the error bar at each conductivity point was from ± 0.0008 mS/cm to ± 0.0226 mS/cm, which indicated the temperature precision was about 0.02 mS/cm. As shown in Fig. 9, the measured conductance (mS) of the five sensor chips showed an excellent linear relationship with the conductivity, with coincided well with the linear regression statistics results. The cell constant K , which denoted the conductivity sensitivity of the proposed sensors, ranging from 2.543 cm^{-1} to 2.592 cm^{-1} , and the average value was 2.559 cm^{-1} , indicating that the sensitivity of the conductivity cell was suitable for measurement in the entire conductivity range (0–101 mS/cm). An excellent linear relationship between the measured (mS) and the predicted (mS/cm) variable for all five conductivity cells with the linear regression coefficient (R^2) ranged from 0.99999 to 1.

Consistency Evaluation of the Conductivity Sensor:

The consistency of the proposed conductivity sensor was assessed through rigorous testing. Two hundred conductance measurements were performed for each of five sensor chips in various KCl solutions.

Standard Deviation and Error:

Cell Constant: The standard deviation of the cell constant among the five chips was $\pm 0.019 \text{ cm}^{-1}$.

Standard Error: The largest standard error ranged from 0.0020 mS/cm at 6.16 mS/cm to 0.0024 mS/cm at 101.00 mS/cm.

Confidence Interval:

95% Confidence Interval: Assuming a Gaussian distribution of measurements, the 95% confidence interval for conductivity measurements was calculated to be $\pm 0.0040 \text{ mS/cm}$ at 6.16 mS/cm and $\pm 0.0048 \text{ mS/cm}$ at 101.00 mS/cm.

Conclusion:

The results demonstrate that the conductivity sensor exhibits exceptional consistency, as evidenced by the low standard deviation of the cell constant and the narrow confidence intervals for conductivity measurements. This high level of consistency makes the sensor well-suited for applications requiring precise and reliable conductivity measurements.

Performance Comparison:**Comparison of the Proposed CT Sensor with Other MEMS-Based Sensors:**

A comparative analysis of the proposed CT sensor with other MEMS-based CT sensors designed for marine measurements is presented in Table I. The following key performance metrics were considered:

Batch Consistency: The proposed CT sensor demonstrated superior batch consistency compared to Broadbent's sensor.

Temperature Precision: The proposed sensor exhibited the highest temperature precision among the compared sensors, attributed to its innovative film platinum resistance design.

Measurement Range: The proposed sensor offers a wider measurement range for conductivity (0-101 mS/cm), enabling data collection and analysis in challenging underwater environments.

These findings highlight the significant advantages of the proposed CT sensor for marine applications, where precise and reliable conductivity and temperature measurements are essential.

CONCLUSION:**Conclusion and Future Directions**

This paper presents a novel MEMS-based conductivity and temperature (CT) sensor, featuring a compact size of approximately $12 \text{ mm} \times 12 \text{ mm}$. The sensor demonstrated exceptional performance in terms of sensitivity, response time, and repeatability for temperature measurements.

Key Achievements:

Batch Consistency: The MEMS-based CT sensors exhibited excellent consistency within a batch, making them suitable for marine monitoring applications.

Experimental Data Contribution: The study provided valuable experimental data for a batch of sensors fabricated for marine measurements.

Future Considerations:

Long-Term Stability: Future research will focus on evaluating the long-term stability of the sensor in real marine environments.

Application Potential:

The proposed CT sensors offer a promising solution for cost-effective sensor nodes in distributed networks for marine environmental monitoring. Their compact size, high performance, and potential for long-term stability make them well-suited for a wide range of marine applications.

REFERENCES:

- [1] D. Duraibabu, G. Leen, D. Toal, T. Newe, E. Lewis, and G. Dooly, "Underwater depth and temperature sensing based on fiber optic technology for marine and fresh water applications," *Sensors*, vol. 17, no. 6, pp. 1228, May 2017.
- [2] E. L. Lewis, "The practical salinity scale 1978 and its antecedents," *Ieee Journal of Oceanic Engineering*, vol. 5, no. 1, pp. 3-8, Jan. 1980.
- [3] J. J. Jijesh, Shivashankar, M. Susmitha, M. Bhanu, and P. Sindhanakeri, "Development of a CTD sensor subsystem for oceanographic application," in *2017 2nd IEEE International Conference on Recent Trends in Electronics, Information & Communication Technology (RTEICT)*, Bangalore, India. 2017, pp. 1487-1492.
- [4] [Online]. Available: <https://www.oceannetworks.ca/innovation-centre/smart-ocean-systems>.
- [5] [Online]. Available: <https://oceanconservancy.org>.
- [6] S. Du, Y. Jia, C. Zhao, G. A. J. Amaratunga, and A. A. Seshia, "A Nail- Size Piezoelectric Energy Harvesting System Integrating a MEMS Transducer and a CMOS SSHI Circuit," *IEEE Sensors Journal*, vol. 20, no. 1, pp. 277-285, Jan. 2020.
- [7] J. Oiler, E. Shock, H. Hartnett, A. J. Dombard, and H. Yu, "Harsh Environment Sensor Array-Enabled Hot Spring Mapping," *IEEE Sensors Journal*, vol. 14, no. 10, pp. 3418-3425, Oct. 2014.
- [8] M. Marcelli, V. Piermattei, A. Madonia, and U. Mainardi, "Design and application of new low-cost instruments for marine environmental research," *Sensors*, vol. 14, no. 12, pp. 23348-23364, Dec. 2014.
- [9] H. A. Broadbent, T. P. Ketterl, A. M. Silverman, and J. J. Torres, "Development of a CTD biotag: Challenges and pitfalls," *Deep-Sea Research Part II-Topical Studies in Oceanography*, vol. 88-89, pp. 131- 136, Apr-May 2013.
- [10] [Online]. Available: <http://www.star-oddi.com>.
- [11] P. M. Ramos, J. M. D. Pereira, H. M. G. Ramos, and A. L. Ribeiro, "A four-terminal water-quality-monitoring conductivity sensor," *Ieee Transactions on Instrumentation and Measurement*, vol. 57, no. 3, pp. 577-583, Mar. 2008.
- [12] M. Asgari, and K. Lee, "Fully-Integrated CMOS Electrical Conductivity Sensor for Wet Media," *IEEE Sensors Journal*, vol. 19, no. 15, pp. 6445- 6451, Apr. 2019.
- [13] M. Crescentini, M. Bennati, and M. Tartagni, "Design of integrated and autonomous conductivity-temperature-depth (CTD) sensors," *AEU - International Journal of Electronics and Communications*, vol. 66, no. 8, pp. 630-635, Aug. 2012.

- [14] M. R. R. Khan, and S. Kang, "Fast, Highly Sensitive Interdigitated Capacitor Sensor to Detect Wide Range of Temperatures Using Graphene-Oxide-Containing Dielectric Membrane," *IEEE Sensors Journal*, vol. 18, no. 7, pp. 2667-2674, Feb. 2018.
- [15] A. Kaidarova, M. Marengo, G. Marinaro, N. Geraldini, C. M. Duarte, and J. Kosel, "Flexible and Biofouling Independent Salinity Sensor," *Advanced Materials Interfaces*, vol. 5, no. 23, pp. 1801110, Oct., 2018.
- [16] A. Nag, S. C. Mukhopadhyay, and J. Kosel, "Sensing system for salinity testing using laser-induced graphene sensors," *Sensors and Actuators A: Physical*, vol. 264, pp. 107-116, Sep. 2017.
- [17] B. Wang, A. Li, S. Yang, and M. Liu, "Strain transfer analysis of surface-bonded MEMS strain sensors," *Chinese Journal of Scientific Instrument*, vol. 13, no. 2, pp. 637-643, Feb. 2013.
- [18] M. Kim, W. Choi, H. Lim, and S. Yang, "Integrated microfluidic-based sensor module for real-time measurement of temperature, conductivity, and salinity to monitor reverse osmosis," *Desalination*, vol. 317, pp. 166-174, May 2013.
- [19] K. Birkelund, A. Hyldgard, D. Mortensen, and E. V. Thomsen, "Miniaturized multi-sensor for aquatic studies," *Measurement Science and Technology*, vol. 22, no. 5, May 2011.
- [20] Y. Zhang, J. L. Cao, Y. Y. Chu, and I. Destech Publicat, "Application Status of MEMS Technology in Marine Field," in *2018 International Conference on Computer, Communication and Network Technology*, Wuzhen, China, 2018, pp. 338-343.
- [21] B. Zhou, C. Bian, J. Tong, and S. Xia, "Fabrication of a Miniature Multi-Parameter Sensor Chip for Water Quality Assessment," *Sensors*, vol. 17, no. 1, pp. 157, Jan. 2017.
- [22] A. Hyldgard, O. Hansen, E. V. Thomsen, and Ieee, "Fish & chips: Single chip silicon mems CTDL salinity, temperature, pressure and light sensor for use in fisheries research," in *18th IEEE International Conference on Micro Electro Mechanical Systems (MEMS)*, Miami Beach, FL, USA, 2005, pp. 303-306.
- [23] A. Hyldgard, D. Mortensen, K. Birkelund, O. Hansen, and E. V. Thomsen, "Autonomous multi-sensor micro-system for measurement of ocean water salinity," *Sensors and Actuators A: Physical*, vol. 147, no. 2, pp. 474-484, Oct. 2008.
- [24] H. A. Broadbent, S. Z. Ivanov, and D. P. Fries, "A miniature, low cost CTD system for coastal salinity measurements," *Measurement Science and Technology*, vol. 18, no. 11, pp. 3295-3302, Nov. 2007.
- [25] H. A. Broadbent, S. Z. Ivanov, and D. P. Fries, "Fabrication of a LCP-based conductivity cell and resistive temperature device via PCB MEMS technology," *Journal of Micromechanics and Microengineering*, vol. 17, no. 4, pp. 722-729, Apr. 2007.
- [26] X. Huang, "In-situ conductivity, temperature, and dissolved oxygen (CT-DO) sensor system for marine measurement," Ph.D. dissertation, Faculty of Physical and Applied Sciences, University of Southampton, Southampton, UK, 2011.
- [27] X. Huang, R. W. Pascal, K. Chamberlain, C. J. Banks, M. Mowlem, and H. Morgan, "A Miniature, High Precision Conductivity and Temperature Sensor System for Ocean Monitoring," *IEEE Sensors Journal*, vol. 11, no. 12, pp. 3246-3252, Dec. 2011.
- [28] H. A. Broadbent, T. P. Ketterl, and C. S. Reid, "A miniature rigid/flex salinity measurement device fabricated using printed circuit processing techniques," *Journal of Micromechanics and Microengineering*, vol. 20, no. 8, Aug. 2010.
- [29] W. G. M. M. K. H. Morgan, "Oceanographic Sensor for in-situ temperature and conductivity monitoring," *OCEANS 2008 - MTS/IEEE Kobe Techno-Ocean*, Kobe, Japan, 2008, pp.1-6.

- [30] G. Keshavaditya, G. R. Eranna, and G. Eranna, "PRT Embedded Micro- Heaters for Optimum Temperature Distribution of Air-Suspended Structures for Gas Sensor Applications," *IEEE Sensors Journal*, vol. 15, no. 7, pp.4137-4140, Jul. 2015.
- [31] A. Hyldgard, K. Birkelund, J. Janting, and E. V. Thomsen, "Direct media exposure of MEMS multi-sensor systems using a potted-tube packaging concept," *Sensors and Actuators a-Physical*, vol. 142, no. 1, pp. 398-404, Mar. 2008.

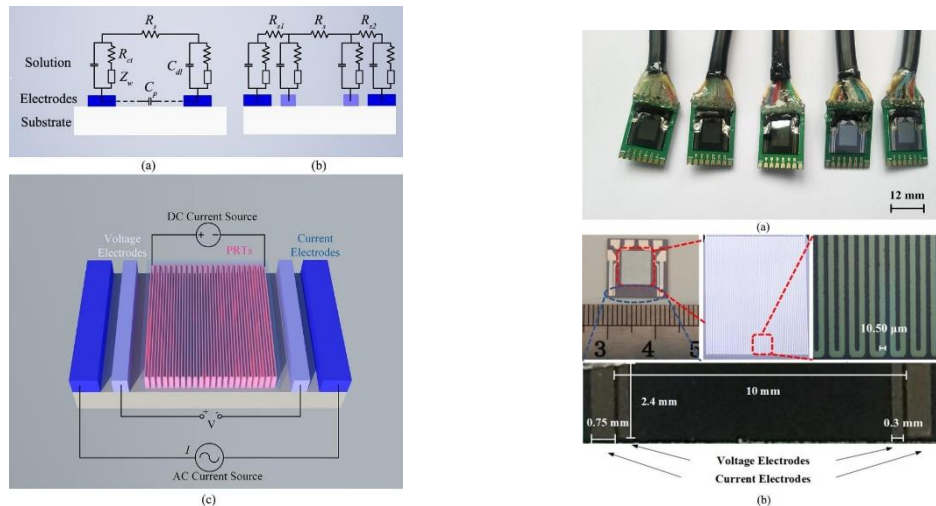


Fig. 1. The equivalent circuits of: (a) two-electrode conductivity cell, and(b) four-electrode conductivity cell; (c) The simplified electrical scheme of the integrated CT sensor. The conductivity cell consists of two voltage electrodes and two current electrodes by injecting the AC current. The temperature sensor can be measured by applying a fixed DC current.

Fig. 2. (a) Photo of the same batch of sensor chips. (b) The thin-film platinum resistance with a width is 10.50 μm is about 5000 Ω at room temperature. The current electrodes have a length of 2.4 mm, and a width of 0.75 mm. The voltage electrodes have a length of 2.4 mm, and a width of 0.3 mm. The spacing between the current electrodes is 10 mm.

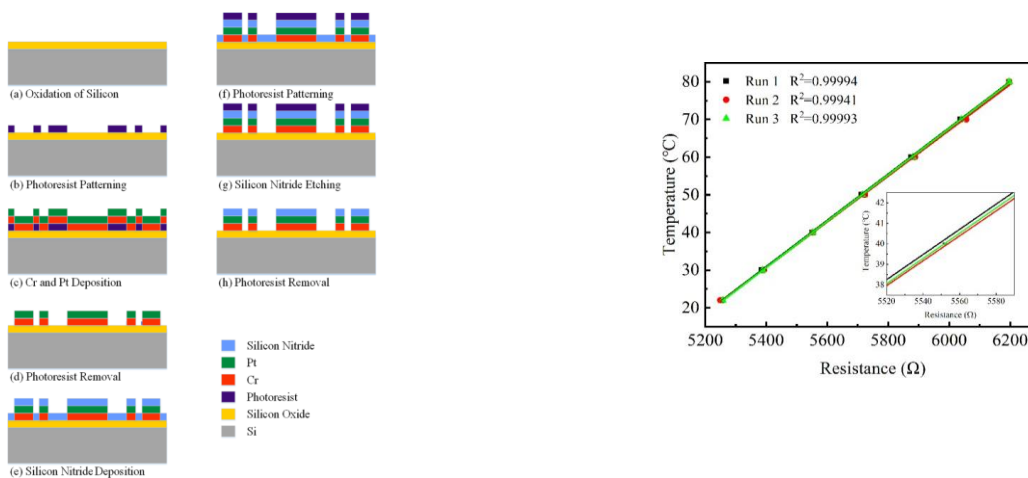


Fig. 3. The batch fabrication process of a CT sensor

Fig. 4. The relationship between resistance and temperature. The calibration procedure was run three times, and the linear relationship between the resistance and temperature with R² values was more than 0.999 for each independent

run. In addition, the film platinum resistance measured at the room temperature was over 5000 Ω , which was larger than that reported in previous literature.

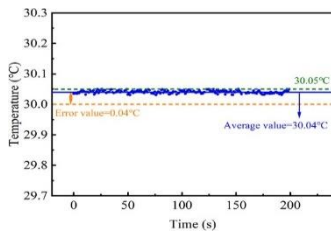


Fig. 5. The temperature sensor was calibrated at the temperature of 30 °C for 200 s.

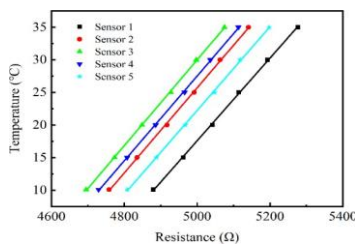


Fig. 6. The linear relationship between the resistance and temperature for the five sensor chips obtained by testing a group of sensor chips at the temperature from 10 °C to 35 °C.

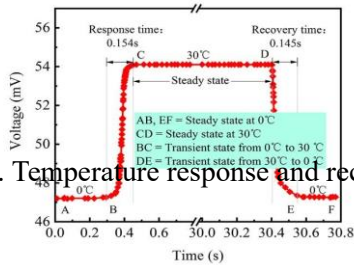


Fig.7. Temperature response and recovery times of the sensor chip.

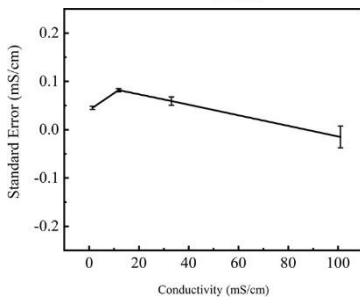


Fig. 8. The measurement error of the conductivity sensor, where the error bar shows the standard deviation of 200 repeated measurements at each temperature point. The maximum measurement error of the conductivity sensor was ± 0.08 mS/cm in the conductivity test from 0 to 101 mS/cm.

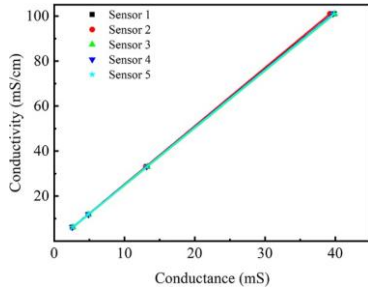


Fig. 9. The linear relationship between the conductance and conductivity for five sensor chips with the linear regression coefficient (R^2) in the range from 0.99999 to 1.

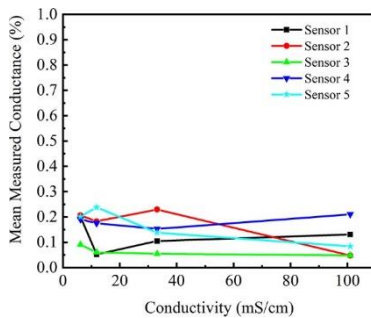


Fig. 10. The variation of the conductance for each sensor chip. In the experiment, 200 conductance measurements were conducted and averaged for each conductivity cell. The standard error of the measurements was calculated and converted to a 95% confidence interval, and expressed as a percentage of the measured conductance.